9.3 TESTS OF TRANSILIENT VERSUS FLUX-GRADIENT TURBULENCE PARAMETERIZATIONS FOR THE PREDICTION OF SURFACE LAYER WIND PROFILES

Robert J. Conzemius*
Windlogics, Inc.
Grand Rapids, Minnesota, USA

1. MOTIVATION AND LAYER OF INTEREST

Turbulence models, based on the Reynolds averaging of the Navier-Stokes equations (RANS) have become the standard for incorporating vertical diffusion of scalars in NWP models. The two most common implementations of turbulence models are the first order models, in which the gradients of horizontally averaged, first-order flow variables are used to predict the eddy exchange coefficients, and 1.5-order, TKE based models, which numerically integrate a prognostic equation for TKE and use the TKE values to calculate eddy exchange coefficients. In both cases, the vertical turbulent fluxes are calculated according to a flux-gradient hypothesis, in which the turbulent fluxes are assumed to be proportional to the negative of the gradient of the mean quantity:

$$\overline{w'\phi'} = -K_\phi \frac{\partial \phi}{\partial z} \quad (1)$$

The flux-gradient hypothesis has long been known to have its shortcomings for applications to the CBL (Deardorff 1966). In particular, counter-gradient fluxes are typically found in the upper portion of the CBL. In order for the model to maintain the flux-gradient relationship (1), the potential temperature profile often shows differences from atmospheric measurements or large eddy simulations (Conzemius and Fedorovich 2004). In particular, the potential temperature gradient is often too strong in the middle CBL, and because the middle-CBL potential temperature is less well-mixed in the vertical, the gradient is too weak in the lower CBL. Similar effects are seen with the profiles of velocity components, with (relative to LES) stronger gradients in the middle CBL and weak gradients in the lower CBL.

* *Corresponding author address:* Robert J. Conzemius, Windlogics, Inc., 201 NW 4th Street, Grand Rapids, MN 55744;
e-mail: bobc@windlogics.com

Some parameterizations have accounted for the counter-gradient fluxes of potential temperature by applying a counter-gradient flux term (e.g. Troen and Mahrt 1986; Hong and Pan 1996), and Moeng and Wyngaard (1989) recommend applying such counter-gradient terms to all CBL scalars. In practice, these terms are usually applied only for the potential temperature turbulent flux.

The differences between actual vertical scalar transport in the CBL and modeled transport in NWP have been attributed to the differences between turbulence modeled as a diffusive process and the advective action of large turbulent structures in the CBL (Stull 1984). Such structures are capable of transporting scalars over a substantial depth, often greater than 1 km (Stull 1984), and the transport may be somewhat different for scalars ascending from the bottom of the CBL versus those descending from the top (Wyngaard and Brost 1984; Moeng and Wyngaard 1989).

Transilient turbulence parameterizations (Stull 1984; Stull 1993) were developed with the hope of accounting for the transport of scalars by coherent, organized structures in the PBL whose vertical extent is generally less than the model grid cell horizontal dimensions but whose vertical extent is often several grid cells deep. Rather than modeling transport as a diffusive process between adjacent grid cells (depending on the order of the numerical scheme), transilient turbulence allows mixing to occur between nonadjacent cells within any given time step, theoretically accounting for the effects of large eddies in the CBL. If these hypotheses are reasonably justifiable, the transilient parameterization should be capable of modeling more realistic CBL scalar profiles than is the case with the more traditional turbulence models.

For the present study, we focus on the transilient approach and compare its predictions of low-level wind and potential temperature profiles to those of the more standard turbulence models employed in NWP. The study will focus

on the dry CBL, and the layer of interest is the upper portion of the surface layer, where Monin-Obukhov similarity theory may or not be applicable, but the velocity gradients are not necessarily weak as might be the case in the mixed layer.

The characterization of low-level wind and potential temperature profiles has obvious impacts on forecasts of wind and temperature. In particular, the wind energy industry relies on accurate predictions of winds in upper surface layer for quantifying the available wind power hours or days in advance of when the power is delivered onto the electrical grid. Additionally, since 0-1 km shear has an impact on the characteristics of deep, moist convection (Doswell and Bosart 2001), it is important for the prediction of sensible weather to accurately characterize low-level profiles. Likewise, many thermally driven flows such as sea breezes and low-level jets are highly sensitive to the turbulence and land-atmosphere exchange processes, and such processes must be well characterized for such flows to be predicted accurately.

2. PARAMETERIZATIONS TESTED

2.1. Mellor-Yamada level 2.5 closure

The Mellor-Yamada level 2.5 closure (Mellor and Yamada 1974, 1982; hereafter denoted as MY2.5) as implemented in the MM5 model (Grell et al. 1994) was tested. The scheme incorporates parameterizations to account for the effects of anisotropy but specifically carries a prognostic equation only for TKE and no other second order moments. It diagnoses turbulence length scales to calculate eddy exchange coefficients. The scheme has been popular in a number of operational NWP models (Janic 1990, 1994; Black 1994).

2.2. MRF PBL parameterization

The second tested parameterization was the MRF scheme (Grell et al. 1994) as implemented in the MM5 model. The scheme uses Richardson-number and velocity scaling criteria to diagnose the PBL depth and then specifies a self-similar profile of eddy exchange coefficients for vertical diffusion over the PBL depth. The PBL depth diagnosis is performed in the same manner for convective, neutral, and stable PBLs, and the same profile of eddy exchange coefficients is used in both cases. The MRF PBL parameterization is described in Troen and Mahrt (1986) and Hong and Pan (1996), and the reader is referred to those articles for a complete description of the scheme. One particular feature of the MRF scheme is its use of a counter-gradient flux term for potential temperature,

$$-\overline{w'\theta'} = K_h\left(\frac{\partial\theta}{\partial z} - \gamma\right), \qquad (2)$$

but this term is not used for any of the other scalars.

2.3. Transilient turbulence based on Richardson number

Transilient turbulence theory is based on the hypothetical nonlocal generalization of (1) (Fiedler 1984)

$$\overline{w'\phi'}(z,t) = \int C(z,z')\frac{\partial}{\partial z'}\phi(z',t)\,dz', \qquad (3)$$

where C is a function describing the potential for mixing between levels z and z'. In the Stull (1984) version of the scheme, the amount of mixing occurring between any two levels i and j in the model grid is dependent on a bulk Richardson number for those two levels:

$$r_{ij} = \frac{g}{\theta_0}\frac{\Delta z_{ij}\Delta\theta_{ij}}{\Delta u_{ij}^2 + \Delta v_{ij}^2}, \qquad (4)$$

where $\Delta\phi_{ij}$ specifies the change in ϕ between i and j. The bulk Richardson number is then used to determine a matrix of coefficients, X_{ij},

$$X_{ij} = 1 - w_{ij}\left[1 - \left(\frac{r_{ij}}{R_T}\right)\right], \qquad (5)$$

where R_T is a termination value for the Richardson number. If $r_{ij}>R_T$, X_{ij} is set equal to 1, and there is no mixing between the i^{th} and j^{th} levels. Additionally, the model does not allow initiation of turbulence between any two levels i and j when the Richardson number is greater than a critical value, R_c. Once turbulence is initiated, it continues until $r_{ij}>R_T$. The weighting factor w_{ij} is given by

$$w_{ij} = \frac{U_0\Delta t}{(j-i)\delta z}, \qquad (6)$$

where U_o is a velocity scale, Δt the time step, and δz is the grid cell vertical dimension. Stull (1984) recommended a velocity scale of U_o=1 m s^{-1}.

The exchange coefficients c_{ij} were then calculated using the constraint

$$\sum_{k=1}^{j-1} c_{ik} - (j-1)c_{ij} = X_{ij}; \quad i < j. \qquad (7)$$

The factor j-1 is applied so that the mixing is more intense near the ground and is reduced at higher levels. The diagonal elements are then calculated so that each row in the exchange matrix sums to unity, and the matrix c_{ij} is symmetrized to ensure conservation of state and mass. It should be noted that a symmetric matrix forces the transilient scheme to obey the same flux-gradient relationship (1) used in the other turbulence closures.

The change of values of the scalar ϕ, due to turbulent mixing, from time step n to time step n+1 is then calculated according to the formula

$$\phi_i^{n+1} = \phi_i^n + c_{ij}\phi_j^n \,. \tag{8}$$

The Prandtl number is assumed to be unity. That is, the same matrix c_{ij} is used for the exchange of all scalars in the CBL. The time tendency of ϕ is

$$\frac{\partial \phi_i}{\partial t} = \frac{\phi_i^{n+1} - \phi_i^n}{\Delta t} \,. \tag{9}$$

For the present analysis, a number of modifications were made. The critical Richardson number R_c, which is necessary for initiating turbulence, was not used in the analysis, because the details of how to implement it in practice were not clear. The turbulence termination value for the Richardson number was taken to be R_T=1. The non-local Richardson number r_{ij} was truncated to fall between r_{ij}=0 and r_{ij}=R_T. The r_{ij}=0 truncation removes occurrences of very large negative r_{ij} when the shear is near zero and the vertical potential temperature gradient is only slightly negative. Such situations can result in unreasonably large variations in X_{ij} when the stability of the atmosphere between i and j is near neutral. The r_{ij}=R_T truncation had the same effect as truncating X_{ij} to be no greater than X_{ij}=1.

Rather than use a fixed velocity scale as in Stull (1984) and Stull (1993), Deardorff (1970) convective velocity scale was used. Additionally, initial tests showed that the gradients of velocity and potential temperature were too weak in the interior of the CBL, so a factor was added to reduce the weights w_{ij} and therefore reduce the mixing. With these changes, the velocity scale was U_o=0.25($B_s z_i$)$^{1/3}$, where B_s is the surface buoyancy flux, and z_i is the boundary layer depth. The boundary layer top was defined in the present analysis as the level where the buoyancy flux reaches its minimum in the entrainment zone.

2.4. Transilient turbulence based on a TKE parameterization

The transilient turbulence model was revised by Stull and Driedonks (1987) to include a parameterization for the effects of TKE. This newer version of the transilient turbulence model is described in the Stull (1993) review paper. A non-local analogy to the TKE equation is used to parameterize the mixing potential between any two levels i and j. A flow-instability contribution to the mixing potential is defined as

$$Y_{ij} = \frac{\Delta t T_o}{\Delta z_{ij}^2}\left(\Delta U_{ij}^2 + \Delta V_{ij}^2 - \frac{g \Delta z_{ij} \Delta \theta_{v,ij}}{\theta_{vo} R_c} \right) - \frac{D_Y \Delta t}{T_o} \,. \tag{10}$$

where $\Delta\theta_{v,ij}$=$\theta_{v,i}$-$\theta_{v,j}$ is the change in potential temperature between levels i and j, ΔU and ΔV are the corresponding changes in velocity components, and Δz_{ij} is the vertical distance between the i and j levels. T_o is a time scale of turbulence, R_c is a critical Richardson number value, g is the acceleration due to gravity, and D_Y is a constant associated with the dissipation of TKE. The diagonal elements of Y are calculated according to the formula

$$Y_{ii} = \max\left(Y_{i,i-1}, Y_{i,i+1}\right) + Y_{ref} \tag{11}$$

where Y_{ref} is a reference value for Y. The recommended values (Stull 1993) for the constants are T_o=1000 s, R_c=0.21, D_Y=1.0, and Y_{ref}=1000.

Once the flow-instability contribution to the mixing potential is calculated, a row norm is then defined:

$$RN_i = \sum_{j=1}^{N} Y_{ij} \,, \tag{12}$$

and an L_∞ matrix norm $\|Y\|_\infty$ by

$$\|Y\|_\infty = \max_i \left(RN_i\right). \tag{13}$$

The matrix of exchange coefficients is then given by

$$c_{ij} = \frac{Y_{ij}}{\|Y\|_\infty} \,, \tag{14}$$

and the diagonal elements of c are

$$c_{ii} = 1 - \sum_{j=1; j\neq i}^{N} c_{ij} \,. \tag{15}$$

The turbulent exchange is then calculated according to (8).

3. LARGE EDDY SIMULATION CASES

Because large eddy simulation resolves most of the energy-containing motions in the turbulent flow, it has become a useful tool for performing tests of RANS-based turbulence

closures using idealized cases. Such LES cases can be designed to focus on one or more particular mechanisms contributing to the evolution of the CBL while eliminating other mechanisms, whose effects the tests are not meant to investigate. The following cases of CBL with wind shears were studied with LES:

1. No mean shear (**NS** case), which was the reference case.
2. Height-constant geostrophic wind of the 20 m/s magnitude throughout the whole simulation domain (**GC** case).

In the **GC** and case, geostrophic wind had only the longitudinal (x) component u_g, so the y component of the geostrophic wind, v_g, was set equal to zero. For all simulated cases, the surface roughness length, geographic latitude, and reference temperature were prescribed to be 0.01 m, 40° N, and 300 K, respectively. Although the **NS** case has no wind, the purpose of including such a case in the present study is to characterize the development of purely convective boundary layers and use it as a null case to investigate the effects of shear-enhanced entrainment (and the model representation thereof) on the wind profiles within shear-driven CBLs.

The virtual potential temperature θ changed vertically at a constant rate of 0.001, 0.003, or 0.010 K/m throughout the entire domain starting from the surface. The initial wind velocity in the domain was geostrophic (zero in the **NS** case), with the vertical velocity component set equal to zero. The surface heat flux had values of 0.03, 0.10, or 0.30 K m s^{-1} and was kept constant with time throughout the run.

The LES grid domain was 5.12×5.12×1.6 km with grid cells of 20 meters in all dimensions. Considering all possible combinations of shear, stratification, and surface heat flux, a total of 16 LES runs were conducted. The combinations with the strongest stratification (0.010 K m^{-1}) and weakest heat flux (0.03 K m s^{-1}) were not conducted due to the excessive time necessary for these cases to run to completion. The LES were allowed to continue until the CBL depth reached approximately 1000 meters, at which point it was possible for the entrainment zone to impinge upon the sponge layer, so the run was stopped. The CBL depth z_i was determined from the minimum of kinematic heat flux $\overline{w'\theta'}$ (resolved + subgrid).

Turbulence statistics were calculated every 100 seconds. The averaging was carried out over the horizontal planes only in order to avoid uncertainties associated with complementary time averaging.

4. MODEL TESTING PROCEDURE

The evaluation of the NWP turbulence closures was carried out in a similar manner to Moeng and Wyngaard (1989) and Ayotte et al. (1996). The LES code was reduced to a one-dimensional column model, and the turbulence closure schemes described in section 2 were inserted into the code. The code was then run for the same period of time as in the LES cases, using the same vertical resolution as the LES grid, and vertical profiles were extracted from the model at a period of time considered to be representative of the CBL evolution.

The Mellor-Yamada level 2.5 closure and the MRF schemes, as used in the MM5 model, use different procedures to calculate surface fluxes of flow variables. In order for test results to be comparable, and for the tests to focus specifically on the characterization of turbulence by each scheme, a consistent method of calculating surface fluxes needed to be applied. Therefore, in all schemes that were tested, the surface potential temperature fluxes were set at constant values specified in section 3. The surface fluxes of velocity components were calculated using Monin-Obukhov similarity theory as was done in LES.

5. RESULTS OF TESTS

Because of the large number of comparisons performed, only the most relevant and representative results are shown. The first case examined was the NS case with a surface heat flux of 0.03 K m s^{-1} and a vertical potential temperature gradient of 0.003 K m^{-1} (Fig. 1). The MY2.5 scheme shows the typical characteristics of the schemes that use the flux-gradient relationship (1). The level of minimum potential temperature is at z=400 m, which is nearly twice as high as what LES predicts. Consequently, the heat content in the lower CBL is larger than predicted by LES. On the other hand, the MRF scheme, which incorporates a counter-gradient flux term, has a potential temperature profile that matches LES very well in the lower CBL and in the surface layer, matches LES most closely. In the upper CBL, its ability to model the simulated potential temperature profile is not as good, but it is not significantly worse than the other models.

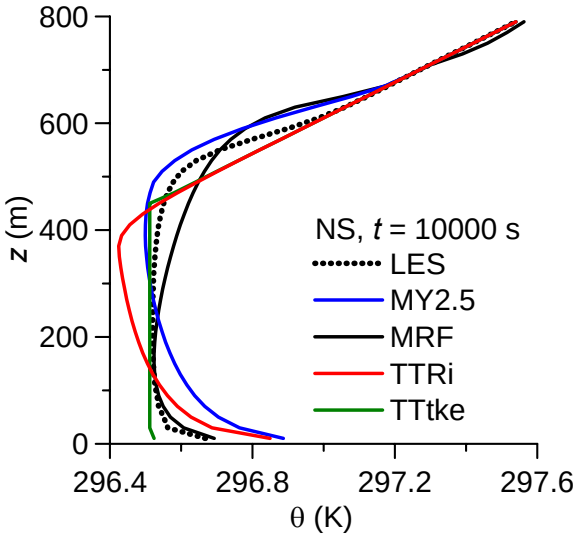

Figure 1. Profiles of potential temperature θ predicted by turbulence closure schemes and LES for the NS case with a surface heat flux of 0.03 K m s^{-1} and a vertical potential temperature gradient of 0.003 K m^{-1}.

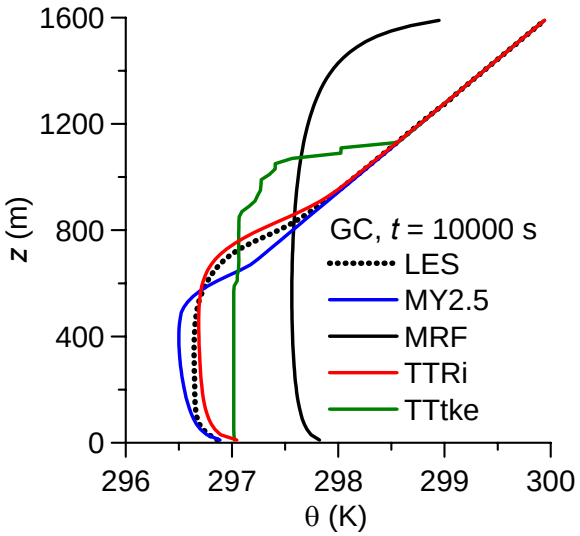

Figure 2. Profiles of potential temperature θ predicted by turbulence closure schemes and LES for the GC case with a surface heat flux of 0.03 K m s^{-1}, a vertical potential temperature gradient of 0.003 K m^{-1}, and a geostrophic wind velocity of u_g = 20 m s^{-1}.

The transilient turbulence schemes as described in section 2, did not predict the temperature profile quite as well for this particular case. The TTtke scheme predicts a very well-mixed profile throughout most of the CBL, including the surface layer, and it has a somewhat unrealistically sharp CBL top. The TTRi scheme predicts potential temperatures that are similar to those predicted by MY2.5 in the surface layer, but it has the coolest of all the potential temperature profiles in the upper CBL, and it also predicts the shallowest CBL depth. Note that the *x*-axis has been displayed in a manner to accentuate the differences among the various schemes. In total, the potential temperature predictions of the four turbulence schemes do not differ very much, but the differences in the CBL depth appear to be rather significant for this case.

The differences are even larger for the GC case with u_g=20 m s^{-1} (Fig. 2). The two local schemes (MRF and MY2.5) show greatly differing potential temperature profiles. The MRF scheme has the most deeply mixed CBL, whereas the MY2.5 has the shallowest. Consequently, the MRF potential temperature in the lower CBL is much higher than predicted by the other models due to the excess entrainment of heat. The TTtke scheme also shows tendencies to have too much entrainment and too deep a CBL. The TTRi scheme matches the LES potential temperature profile very closely.

The reason for the excessively deep CBL depths predicted by the MRF in this case is due to its diagnosis of the PBL depth. The first guess of the PBL depth is determined by the level at which a bulk Richardson number, dependent on mean flow, parameters, exceeds a critical value of 0.5. The Richardson number is defined as

$$\mathrm{Ri}_B = \frac{g}{\theta_{vo}} \frac{\left(\theta_v - \theta_{vs}\right)}{\left(U^2 + V^2\right)}, \qquad (16)$$

where θ_v is the virtual potential temperature, θ_{vo} its reference value, θ_{vs} is the virtual potential temperature of the lowest above-ground model level, and *U* and *V* are the velocity components. In the dry CBL cases presented here, the virtual potential temperature can be considered identical to the potential temperature. The initial PBL height is then enhanced by considering the initial TKE a thermal, rising from the surface layer, might have given the surface fluxes there. In the GC cases, since *U*=20 m s^{-1} initially, the scheme immediately diagnoses a very deep PBL depth, regardless of the turbulence that has actually developed. Although the initial condition in the GC cases considered here might be somewhat unrealistic in that the wind is in geostrophic balance all the way down to the lowest level of *z*=10 m, the effects are, nevertheless, clear.

Interestingly, this characteristic of the MRF does not greatly affect its prediction of the low-level wind profiles (Fig. 3). It appears that, due

to the excessively deep PBL, the downward mixing of momentum compensates for a decrease of momentum that is inherent with the schemes that obey the flux-gradient relationship (1). The MY2.5 scheme shows the more typical profile. The gradients of U are too strong in the middle CBL and too weak in the surface layer. Although its velocity at z=10 m does not differ much from LES, the weak gradients in the upper surface layer cause the wind speeds to be too slow there.

The slowing of the x-component of the wind from its geostrophic value results in the development of a positive y-component, due to the effects of the Coriolis force. Figure 4 shows the y-component of velocity at t=10000 s. The MY2.5 scheme happens to match the LES values most closely at this selected time. Otherwise, the models show some rather large differences in predicted V values, and the predictions of CBL depth are primarily responsible for the differences in these values. The MRF scheme develops the deepest CBL, and the depth over which the modeled winds depart from their geostrophic values is much greater than in the other models. In the case of the TTtke scheme, the excessive downward mixing of momentum to the surface causes increased surface drag, decreasing the x-component of the wind and increasing the y-component more than is the case with the other models. Such differences in CBL depth, mixing, and departures of the wind from geostrophic values has significant implications for predictions of wind during later times in the model run.

Figure 5 shows the evolution of the wind speed at z=80 m, which is a typical height of wind turbine hubs. The LES speeds are generally the fastest. It must be noted that LES does not necessarily reproduce the evolution of the surface layer winds with a great deal of accuracy. The resolution of turbulent motions is very poor in the surface layer, and the turbulent component of the flow is primarily relegated to the subgrid model. LES comparison exercises (Fedorovich et al. 2004) have shown that the horizontally averaged wind speeds in the upper surface layer, with a couple exceptions, differed by approximately 0.5 m s^{-1} or less for a case very similar to the GC case shown in the present study.

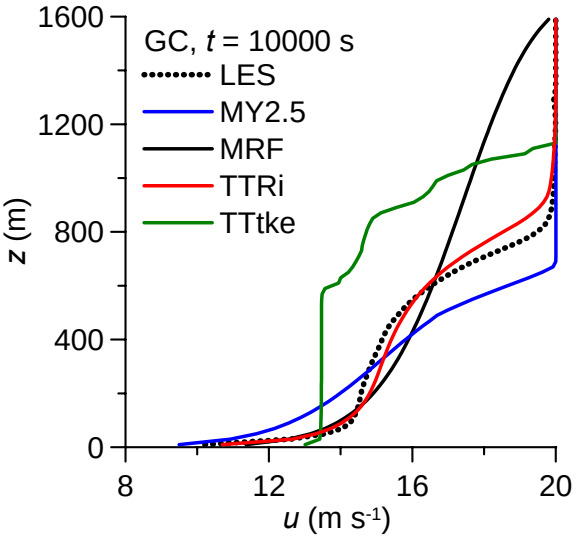

Figure 3. Profiles of the x-component of velocity predicted by turbulence closure schemes and LES for the GC case with a surface heat flux of 0.03 K m s^{-1}, a vertical potential temperature gradient of 0.003 K m^{-1}, and a geostrophic wind velocity of u_g = 20 m s^{-1}.

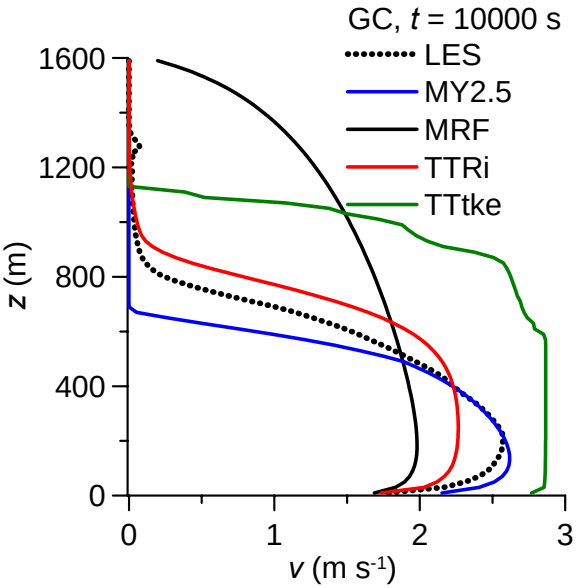

Figure 4. Profiles of the y-component of velocity predicted by turbulence closure schemes and LES for the GC case with a surface heat flux of 0.03 K m s^{-1}, a vertical potential temperature gradient of 0.003 K m^{-1}, and a geostrophic wind velocity of u_g = 20 m s^{-1}.

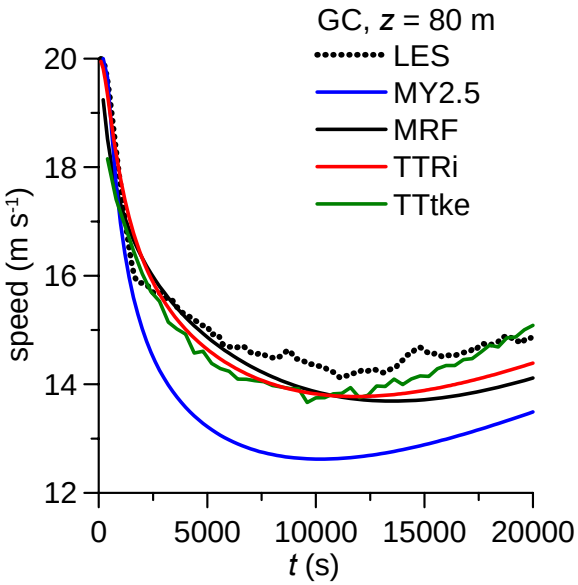

Figure 5. Predictions of the wind speeds at z=80 m, as a function of time t, for the GC case shown in Figs. 2, 3, and 4.

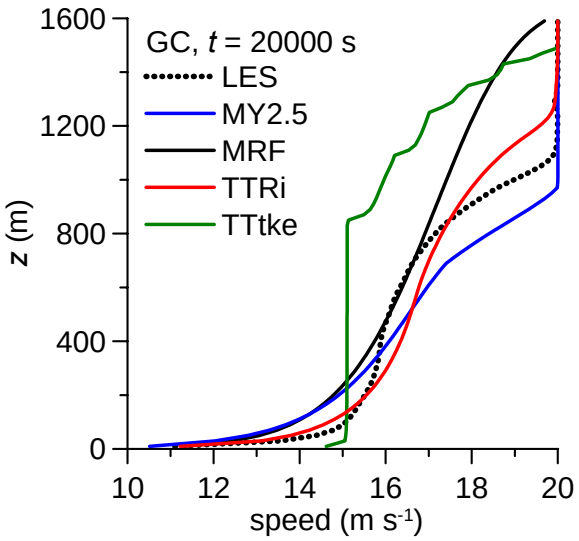

Figure 6. Profiles of wind speed predicted by turbulence closure schemes and LES at t=20000 s for the GC case shown in Figs. 2-5.

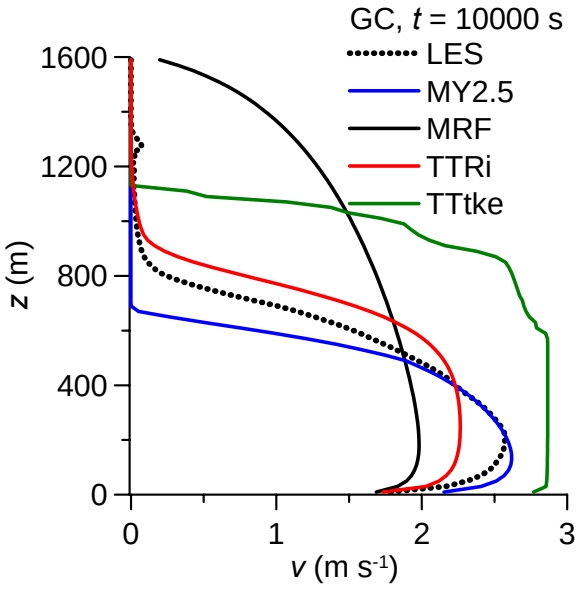

Figure 7. Profiles of the y-component of velocity predicted by turbulence closure schemes and LES at t=20000 s for the GC case shown in Figs. 2-6.

Otherwise, the models show some rather significant differences in the wind speeds. The MY2.5 scheme produces the slowest speeds due to its characteristic gradients shown in Figs. 3 and 4. Despite this problem, the MY2.5 shows what, perhaps, is the best evolution of the CBL in terms of its bulk characteristics, such as CBL depth and integral potential temperature and velocity. The MRF scheme, despite its poor prediction of the CBL evolution, reproduces the simulated wind speed rather well throughout the early portion of the simulation, but it eventually predicts wind speeds that are slower than LES.

The two transilient turbulence schemes do the best overall in terms of matching the simulated speeds. The TTRi version tends to match the time tendencies shown in LES, but the TTtke version matches LES better, despite its relatively poor predictions of CBL integral properties (Figs 2, 3, and 4). Note the time tendency of the wind speeds predicted by TTtke between t=10000 s and t=20000 s does not match that of LES particularly well.

For further investigation into the causes for the different wind speed predictions during the latter portions of the simulated case, Figures 6 and 7 show the wind speed and y-component of the mean flow, respectively, for t=20000 s. The TTtke scheme, despite its more accurate predictions of the simulated speeds at z=80 m, actually matches LES relatively poorly over most of the depth of the CBL. Looking at Figs. 6 and 7, it appears that the MY2.5 and TTRi schemes predict the simulated flow better than the other schemes when the schemes are compared in an integral sense. These two schemes tend to match each other relatively closely overall. However, the differences in predicted z=80 m wind speeds are rather substantial (Fig. 5), and Fig. 6 shows why. The MRF and MY2.5 schemes display the common behavior of predicting vertical gradients in wind speed that

are too weak in the surface layer. Thus, the wind speed predictions may be relatively accurate at z=10 m, where the lower boundary condition (M-O similarity) is applied, but the speeds are too slow in the upper portions of the surface layer.

6. CONCLUSIONS AND FUTURE WORK

Turbulence closure schemes that obey the flux gradient hypothesis (1) in predicting vertical fluxes of scalars predict wind speeds that are characteristically slower than LES-predicted speeds in the upper portion of the surface layer. These slow speeds are associated with velocity gradients in the middle CBL that are required to maintain downward fluxes in such models, whereas LES shows that the vertical gradients of velocity can be much weaker. Although bulk velocity profiles might be nearly correct in an integral sense (such as in the MY2.5 closure), the presence of gradients, in the middle CBL, that are stronger than simulated gradients, causes the models to predict weaker gradients and slower speeds in the surface layer.

The transilient turbulence models alleviate this problem somewhat by enhancing the exchange of scalars in the middle CBL. However, there are certain hypotheses inherent in transilient models that do not make sense physically. In particular, the depth of the non-local exchange of scalars among grid levels can exceed what is physically possible in a single model time step. Typical vertical velocity in the CBL is on the order of 1 m s^{-1}, and typical CBL depths are on the order of 1000 m. The turbulence time scale is therefore approximately 1000 s, yet scalars can easily be transported over the entire CBL depth in a model time step of only one second. Although the primary exchange still occurs between adjacent levels, transport over larger distances, however minor, in such short periods of time makes the non-local exchange hypothesis (2) rather difficult to accept.

Further tests of the transilient models might utilize a Prandtl number that is different from unity. This may reduce some of the differences between the profiles of potential temperature in the transilient models versus LES, seen in Fig. 1. Nevertheless, the symmetrization of the matrix of exchange coefficients c_{ij} relegates the transilient model to a flux-gradient type model, in which the relationship (1) is maintained. This makes it impossible for the transilient models to reproduce the counter-gradient fluxes in LES.

The profiles and fluxes, predicted by LES in the surface layer, need to be compared to those predicted by Monin-Obukhov (M-O) similarity theory. Although M-O theory is applied at the lowest grid level, both in LES and in NWP, the simulations and models control the fluxes and gradients everywhere above that point, even though M-O theory may be applicable over a deeper layer. Consequently, there is no guarantee that the simulated profiles will obey M-O theory over the entire depth where the theory is valid and well-tested.

There are alternative, possibly better methods to address problems with the surface layer wind predictions. In particular, Moeng and Wyngaard (1989) recommend applying a counter-gradient term (like that applied in MRF), to all scalars in the CBL. This term accounts for the differences in top-down and bottom-up scalar diffusion that are not taken into account in most RANS-based turbulence models (Wyngaard and Brost 1984). Alternatively, higher order turbulence modeling can be incorporated into NWP. However, the relatively high numerical cost and additional assumptions necessary to develop such schemes makes their implementation in NWP models rather difficult. Thirdly, one may simply wait for the horizontal resolution in NWP to become fine enough that CBL turbulent motions are resolved on the model grid. Presently, some mesoscale NWP models are beginning to reproduce some CBL structures in grids as fine as 1 km (Xue and Martin 2006a, 2006b). However, such modeling falls into the “terra incognita” (Bryan et al. 2003) in which neither the RANS-based nor the LES subgrid turbulence models were intended to be applied.

7. REFERENCES

Ayotte, K. W., P. P. Sullivan, A. Andren, Scott C. Doney, A. A. M. Holtslag, W. G. Large, J. C. McWilliams, C.-H. Moeng, M. J. Otte, J. J. Tribbia, and J. C. Wyngaard, 1996: An evaluation of neutral and convective planetary boundary-layer parameterizations relative to large eddy simulations. *Bound. Layer Meteorol.,* **79,** 131-175.

Black, T. L., 1994: The new NMC mesoscale Eta model: description and forecast examples. *Wea. and Forecast.,* **9,** 265-278.

Bryan, G. H., J. C. Wyngaard, and J. M. Fritsch, 2003: Resolution Requirements for the Simulation of Deep Moist Convection. *Mon. Wea. Rev.,* **131,** 2394–2416.

Conzemius, R. and E. Fedorovich, 2004: Numerical models of entrainment into sheared convective boundary layers evaluated through large eddy simulations. Preprints, *16th Symp. on Boundary Layers and Turbulence*, Amer. Meteor. Soc., 9-13 August, Portland, Maine, USA, CD-ROM, 5.6.

Deardorff, J. W., 1966: The Counter-Gradient Heat Flux in the Lower Atmosphere and in the Laboratory. *J. Atmos. Sci.,* **23,** 503–506.

Deardorff, J. W., 1970b: Convective velocity and temperature scales for the unstable planetary boundary layer and for Raleigh convection. *J. Atmos. Sci.*, **27**, 1211-1213.

Doswell, C. A. III, and L. F. Bosart, 2001: Extratropical synoptic-scale processes and severe convection. *Severe Convective Storms.* American Meteorological Society, 561 pp.

Fedorovich, E., R. Conzemius, I. Esau, F. Katapodes-Chow, D. Lewellen, C.-H. Moeng, P. Sullivan, D. Pino, and J. V.-G. de Arellano, 2004c: Entrainment into sheared convective boundary layers as predicted by different large eddy simulation codes. *Proc. 16th Symp. On Boundary Layers and Turbulence,* Portland, Maine, U.S.A.

Fiedler, B. H., 1984: An integral closure model for the vertical turbulent flux of a scalar in a mixed layer. J. Atmos. Sci., 41, 674-680.

Fiedler, B. H., and F. Kong, 2003: The performance of an *E-l* scheme for the atmospheric boundary layer in a mesoscale model with grid spacing as small as 1 km. *Meteorol. Atmos. Phys.,* **84,** 1-10.

Grell, G. A., J. Dudhia, and D. R. Stauffer, 1994: A description of the Fifth-generation Penn State/NCAR mesoscale model (MM5). NCAR Technical Note, NCAR/TN-98+STR, 117 pp.

Hong, S.-Y. and H.-L. Pan, 1996: Nonlocal Boundary Layer Vertical Diffusion in a Medium-Range Forecast Model. *Mon. Wea. Rev.,* **124,** 2322–2339.

Janjic, Z. I., 1990: The step-mountain coordinate: physical package. *Mon. Wea. Rev.,* **118,** 1429-1443.

Janjic, Z, 1994: The step-mountain eta coordinate model: further developments of the convection, viscous sublayer, and turbulence closure schemes. *Mon. Wea. Rev.,* **122,** 927-945.

Mellor, G. L., and T. Yamada, 1974: A hierarchy of turbulence closure models for planetary boundary layers. *J. Atmos. Sci.,* **31,** 1791-1806.

Mellor, G. L., and T. Yamada, 1982: Development of a turbulence closure model for geophysical fluid problems. *Rev. Geophys. Space Phys.,* **20,** 851-875.

Moeng, C.-H. and J. C. Wyngaard, 1989: Evaluation of turbulent transport and dissipation closures in second-order modeling. *J. Atmos. Sci.,* **46,** 2311-2330.

Stull, R. B., 1984: Transilient turbulence theory. Part I: the concept of eddy-mixing across finite distances. *J. Atmos. Sci.,* **41,** 3351-3367.

Stull, R. B., 1993: Review of non-local turbulent mixing in turbulent atmospheres: transilient turbulence theory. *Bound. Layer. Meteor.,* **62,** 21-96.

Stull, R. B., and T. Hasagawa, 1984: Transilient turbulence theory. Part II: Turbulent adjustment. *J. Atmos. Sci.,* **41,** 3368-3379.

Stull, R.B. and A.G.M. Driedonks, 1987: Applications of the transilient turbulence parameterization to atmospheric boundary layer simulations. *Bound.-Layer Meteor.,* **40,** 209-239.

Troen, I., and L. Mahrt, 1986: A simple model of the atmospheric boundary layer; sensitivity to surface evaporation. *Bound.-Layer Meteor.,* **37,** 129-148.

Wyngaard, J. C., and R. A. Brost, 1984: Top-down and bottom-up diffusion of a scalar in the convective boundary layer. *J. Atmos. Sci.,* **41,** 102-112.

Xue, M., and W. J. Martin, 2006: A High-Resolution Modeling Study of the 24 May 2002 Dryline Case during IHOP. Part I: Numerical Simulation and General Evolution of the Dryline and Convection. *Mon. Wea. Rev.,* **134,** 149–171.

Xue, M., and W. J. Martin, 2006: A High-Resolution Modeling Study of the 24 May 2002 Dryline Case during IHOP. Part II: Horizontal Convective Rolls and Convective Initiation. *Mon. Wea. Rev.,* **134,** 172–191.